remote sensing

MDPI

Article

Watch Out for the Tailings Pond, a Sharp Edge Hanging over Our Heads: Lessons Learned and Perceptions from the Brumadinho Tailings Dam Failure Disaster

Deqiang Cheng [1], Yifei Cui [2,*], Zhenhong Li [3,4,5] and Javed Iqbal [6,7,8]

1 Key Research Institute of Yellow River Civilization and Sustainable Development & Collaborative Innovation Center on Yellow River Civilization Jointly Built by Henan Province and Ministry of Education, Henan University, Kaifeng 475001, China; 10340052@henu.edu.cn
2 State Key Laboratory of Hydroscience and Engineering, Tsinghua University, Beijing 100084, China
3 College of Geological Engineering and Geomatics, Chang'an University, Xi'an 710054, China; zhenhong.li@chd.edu.cn
4 Key Laboratory of Western China's Mineral Resource and Geological Engineering, Ministry of Education, Xi'an 710054, China
5 Big Data Center for Geosciences and Satellites (BDCGS), Xi'an 710054, China
6 Key Laboratory of Mountain Hazards and Earth Surface Process, Institute of Mountain Hazards and Environment, Chinese Academy of Sciences, Chengdu 610041, China; javediqbalgeo@uoh.edu.pk
7 Department of Earth Sciences, The University of Haripur, Haripur 22620, Pakistan
8 China-Pakistan Joint Research Centre on Earth Sciences, Chinese Academy of Sciences, Islamabad 45320, Pakistan
* Correspondence: yifeicui@mail.tsinghua.edu.cn; Tel.: +86-010-62788585

Citation: Cheng, D.; Cui, Y.; Li, Z.; Iqbal, J. Watch Out for the Tailings Pond, a Sharp Edge Hanging over Our Heads: Lessons Learned and Perceptions from the Brumadinho Tailings Dam Failure Disaster. *Remote Sens.* **2021**, *13*, 1775. https://doi.org/10.3390/rs13091775

Academic Editors: Paolo Mazzanti and Saverio Romeo

Received: 18 January 2021
Accepted: 26 April 2021
Published: 2 May 2021

Abstract: A catastrophic tailings dam failure disaster occurred in Brumadinho, Brazil on 25 January 2019, which resulted in over 270 casualties, 24,000 residents evacuated, and a huge economic loss. Environmental concerns were raised for the potential pollution of water due to tailings waste entering the Paraopeba River. In this paper, a detailed analysis has been carried out to investigate the disaster conditions of the Brumadinho dam failure using satellite images with different spatial resolutions. Our in-depth analysis reveals that the hazard chain caused by this failure contained three stages, namely dam failure, mudflow, and the hyperconcentrated flow in the Paraopeba River. The variation characteristics of turbidity of the Rio Paraopeba River after the disaster have also been investigated using high-resolution remote sensing images, followed by a qualitative analysis of the impacts on the downstream reservoir of the Retiro Baixo Plant that was over 300 km away from the dam failure origin. It is believed that, on the one hand, the lack of dam stability management at the maintenance stage was the main cause of this disaster. On the other hand, the abundant antecedent precipitation caused by extreme weather events should be a critical triggering factor. Furthermore, the spatiotemporal pattern mining of global tailings dam failures revealed that the Brumadinho dam disaster belonged to a Consecutive Hot Spot area, suggesting that the regular drainage inspection, risk assessment, monitoring, and early warning of tailings dam in Consecutive Hot Spot areas still need to be strengthened for disaster mitigation.

Keywords: hazard chain; turbidity; suspended sediment detection; extreme climate events; tailing dam risk management; spatiotemporal pattern mining; El Niño

1. Introduction

Tailings are the material left after the valuable parts have been separated from the uneconomic or low-economic ore. A tailings dam is typically an earth-fill embankment dam which is usually designed for permanent containment by intercepting valleys or enclosing lands in order to form a tailings pond used to store metal or non-metal ore-separation and discharging tailings or other industrial waste residues. Consequently, the

tailings dam is a dangerous source of man-made mudflow with high potential energy. The failure of the tailings dam is one of the most dangerous disasters causing serious accidents. Tailings dams are considered more vulnerable than hydraulic dams due to the lack of regulations on specific design criteria, stability requirements regarding monitoring during the construction and maintenance process, and high potential of pollution due to its filled material (solid waste) [1].

The mining byproducts collected in tailings dams may damage the environment by releasing toxic metals and poisoning the aquatic wildlife that relies on clear water [2]. In past decades, many researchers have investigated tailings dam failures using different research methods, e.g., site investigation, numerical simulation, and remote sensing technology. A field investigation has been proven to be a good method to obtain first-hand data when accessibility is possible to the disaster site. For example, Macklin et al. [3] collected sediment samples affected by tailings dam failures to assess the long-term fate and environmental significance of contaminant metals. Porsani et al. [4] used Ground-Penetrating Radar (GPR) on an iron mining area after the collapse of the tailings dam I at the Córrego do Feijão Mine in Brumadinho-MG, Brazil to map bodies, structural buildings, and equipment buried in the mud. A numerical simulation is another effective means, which can help us understand the tailing flow characteristics and assess the possible extents of the affected areas [5,6]. With the advance in remote sensing technology, remote sensing has been becoming a more and more important means of information acquisition in disaster investigation [7–10]. Many scholars have applied remote sensing technology to the study of tailings dam failure disasters. For example, Silveira et al. [11] used semivariogram indices derived from NDVI images to obtain an object-based change detection caused by the Mariana dam disaster. Grenerczy and Wegmüller [12] performed a Persistent Scatterer InSAR (PSI) analysis to examine the embankment failure of a red mud reservoir. The tailings dam failure is a kind of disaster which could affect wide areas, especially those along rivers, and different disaster characteristics often appear in different regions. Therefore, different remote sensing techniques are usually requested to be employed to analyze a series of remote sensing images to reflect the whole disaster process. In this study, we attempt to make full use of the available remote sensing images to examine the Brumadinho tailings failure disaster in order to make people realize the great harm of tailings dam failures. In addition, this paper demonstrates how RS techniques can be used to characterize and monitor the evolution of such complex processes, which provides a reference for disaster prevention and mitigation.

2. Background of the Brumadinho Tailings Dam Failure Disaster

Brumadinho is a Brazilian municipality, located near the Paraopeba River at an altitude of 880 m. It belongs to the microregion of Belo Horizonte, Metropolitana de Belo Horizonte, Minas Gerais, Brazil (Figure 1). Just after noon on 25 January 2019, the Brumadinho dam disaster occurred when Dam I (Figures 2 and 3), a tailings dam at the Córrego do Feijão iron ore mine owned by Vale, 9 km (5.6 mi) east of Brumadinho (Figure 1b), suffered a catastrophic failure [13].

Figure 1. Location of Brumadinho dam disaster. (**a**) Location of the disaster in Brazil; (**b**) relative relationship between the disaster location and two reservoirs. Note that in Figure 1b, the position of two reservoirs were marked using a red box whose extent corresponds to Figure 9a.

Figure 2. Video screenshots of the Brumadinho tailings dam failure [14]; (**a**) 25 January 2019, 12:28:21; (**b**) 25 January 2019, 12:28:36; (**c**) 25 January 2019, 12:28:43; (**d**) 25 January 2019, 12:28:52 (local time).

In this disaster, at least 248 people were confirmed dead, and 22 missing. Most of the victims were Vale's employees. At a railroad branch, in the Córrego do Feijão region, three locomotives and 132 wagons were buried, and four railway men were missing. Two sections of the railway bridge (Figure 3) and about 100 m of railway track were also struck and destroyed by the mud [15]. Due to the potential hazards, about 24,000 residents from several districts of Brumadinho were evacuated [16]. Many agricultural areas were affected or totally destroyed, and the local livestock industry suffered damages due to the loss of animals such as cattle and poultry [17]. In addition, the tailings dam failure spilt about 12 million cubic meters of mud and sludge [18] and some came into and ran along the

Paraopeba River. The metals in the tailings may be adsorbed by the river sediments or may pollute the soil in the floodplain, and would end up affecting the region's ecosystem.

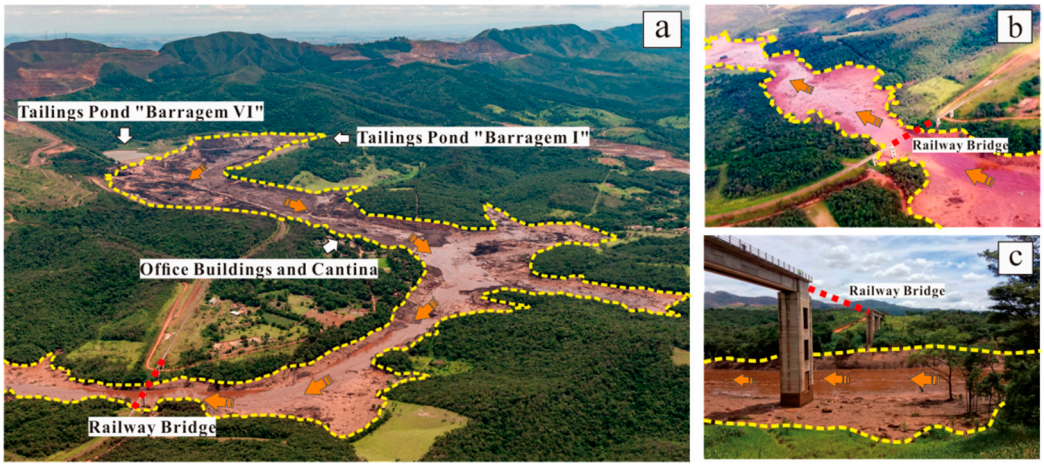

Figure 3. Disaster pictures. (**a**) Aerial view of Brumadinho dam disaster taken at 11:46 on 27 January 2019 [19]; (**b**) video screenshot of the destroyed railway bridge, 3 km downstream from the collapsed dam, on 26 January 2019 from YouTube [20]; (**c**) picture of iron ore railway bridge destroyed by mudflow taken on 26 January 2019 [21]. Note that the yellow line represents the extents of the areas affected by the mudflow, the red line represents the railway bridge which was damaged, and the brown arrow indicates the movement direction of the mudflow.

3. Materials and Methods

3.1. Materials

3.1.1. High-Resolution Remote Sensing Images

Freely available remote sensing (RS) imagery can be used to investigate natural hazards such as landslides [9,22], debris flows [8,9] and mountain fires [23]. Google Earth is an important open source of high-resolution remote sensing imagery, and more importantly, it can provide multi-temporal remote sensing datasets [24–26]. In this study, seven high-resolution remote sensing images from Google Earth were used to track the movement of sediment in the channel after the tailings entered the Paraopeba River: Three images at the confluence of the debris flow gully and the Paraopeba River (collected at different times), one image at the stage of sediment transport in the river, and three others covering the area where the river enters the Retiro Baixo reservoir (different times).

3.1.2. Medium-Resolution Remote Sensing Images

Landsat satellite images of National Aeronautics and Space Administration (NASA) are important medium-resolution image datasets that can be used to investigate natural hazards. Landsat 8, as an American Earth observation satellite, is the eighth satellite launched on 11 February 2013 in the Landsat program. It has two sensors including the Operational Land Imager (OLI) and the Thermal Infrared Sensor (TIRS). The OLI consists of 8 bands with a spatial resolution of 30 m, and a 15-m panchromatic band. The TIRS can provide 100-m thermal infrared images.

In this study, Landsat 8 images were used to investigate the hazard chain. They were true color synthesized images of the pre- and post-disaster and released by the researchers of NASA without copyright protection [27,28]. Landsat 8 images were also used to examine the sediment concentration of pre- and post-disaster in the reservoirs. Three Landsat 8 images of the pre- and post-disaster (Table 1) were downloaded from the USGS Global Visualization Viewer (GloVis) website [29], and used to examine the diffusion of waste in the reservoirs of two hydroelectric plants.

Table 1. Landsat 8 remote sensing images used for the examination of sediment concentration [29].

Type	File Name	Resolution	Date
Pre-disaster	LC08_L1TP_219073_20181220_20181227_01_T1	15/30/100 m (panchromatic/multispectral/thermal)	20 December 2018
Post-disaster	LC08_L1TP_219073_20190222_20190222_01_RT	15/30/100 m (panchromatic/multispectral/thermal)	22 February 2019
	LC08_L1TP_219073_20190427_20190508_01_T1	15/30/100 m (panchromatic/multispectral/thermal)	27 April 2019

3.1.3. Global Tailings Dam Failures Database

There are about 3500 active tailings ponds in the world, among which 2000 experience about two to five known "major" failures, and 35 "minor" failures annually [30]. During the period from 2007 to 2017, there were at least 10 very serious mine tailings dam failures involving multiple loss of life, with approximately 20 lives per incident, a release of at least 1 million cubic meters of waste each time, and a travel of 20 km or longer every waste movement [31]. Based on the world mine tailings failure data with more than 300 records during the period from 1915 to 2019 [14], a global spatial geographic database of tailings dam failure was made using ArcGIS. Using the "Natural Break" classification method, the tailings dam failure records could be divided into five categories (Figure 4).

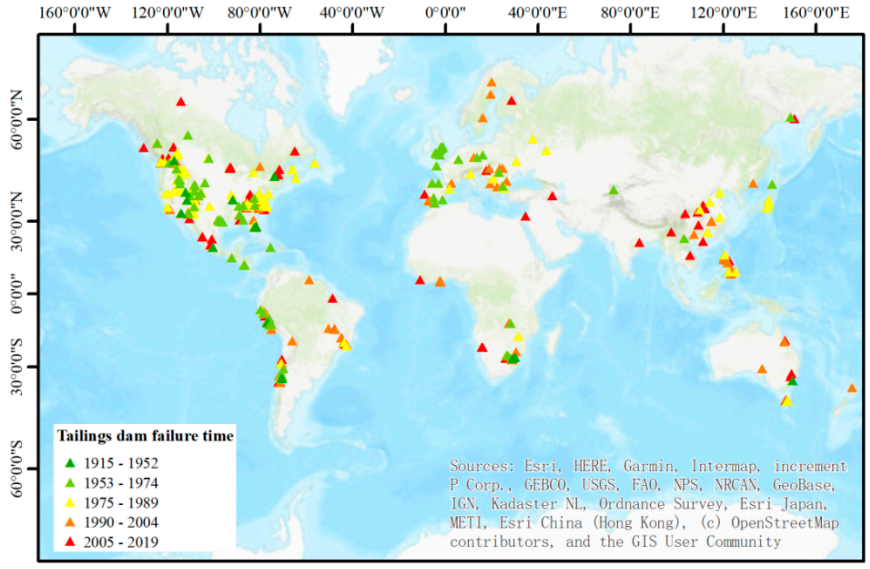

Figure 4. Tailings dam failures (1915–2019) with their occurrence times.

3.2. Methods

3.2.1. FLAASH Atmospheric Correction and Remote Sensing Image Fusion

Solar radiation needs to pass through the atmosphere before it is collected by satellites [32]. Due to this, remote sensing images include complex information derived from the atmosphere and the Earth's surface. As this research is focused on the quantitative analysis of surface reflectance, we need to mitigate the influence from the atmosphere. Using the Atmospheric Correction Module, we can compensate for atmospheric effects.

Atmospheric correction can be realized using many available software tools. For example, the Atmospheric Correction Module in the ENVI software [33] provides two atmospheric correction modeling tools for retrieving spectral reflectance from multispectral and hyperspectral radiance images: Quick Atmospheric Correction (QUAC) and Fast Line-of-sight Atmospheric Analysis of Spectral Hypercubes (FLAASH). The accuracy of FLAASH model is higher than that of QUAC model. The application of QUAC model is simpler than that of FLAASH, and it has less dependence on input parameters and

calibration accuracy of instruments [34,35]. FLAASH is a first-principle atmospheric correction tool that corrects wavelengths in the visible through near-infrared and shortwave infrared regions. In this study, the atmospheric correction of Landsat images was carried out using the FLAASH tool within the ENVI software [36].

Image fusion in remote sensing has several application domains. An important domain is multi-resolution image fusion [37]. Many different multi-resolution image fusion methods are available with different characteristics [38], including Gram–Schmidt Pan Sharpening [39], HSV Transformation [40], and Brovey Transformation [41]. Using these image fusion methods, important information from multiple images can be gathered together to form a new image with both high spatial resolution and multispectral characteristics. The OLI has two types of images including panchromatic images and multispectral images. On the basis of comparing different methods, we selected the Gram–Schmidt Pan Sharpening method to fuse images due to its superiority to maintain spatial texture information, especially to keep spectral features with high fidelity [42].

3.2.2. Waterbody Extraction

In order to carry out the research of suspended sediment information in the reservoirs, it is necessary to obtain an accurate extent of the reservoirs. Due to the water spectral characteristics of the near-infrared band absorbing strongly, but reflecting highly in the green band (Figure 5), the Normalized Difference Water Index (NDWI) was proposed by Mcfeeters [43] as follows:

$$\text{NDWI} = (\text{Green} - \text{NIR})/(\text{Green} + \text{NIR}) \quad (1)$$

where Green and NIR are reflectance factors in green and near-infrared bands, corresponding to Bands 3 and 5 of Landsat 8 imagery. After calculating the NDWI, we used 0 as the segmentation threshold to extract the water body, and the water body boundaries were manually extracted in the ArcGIS software.

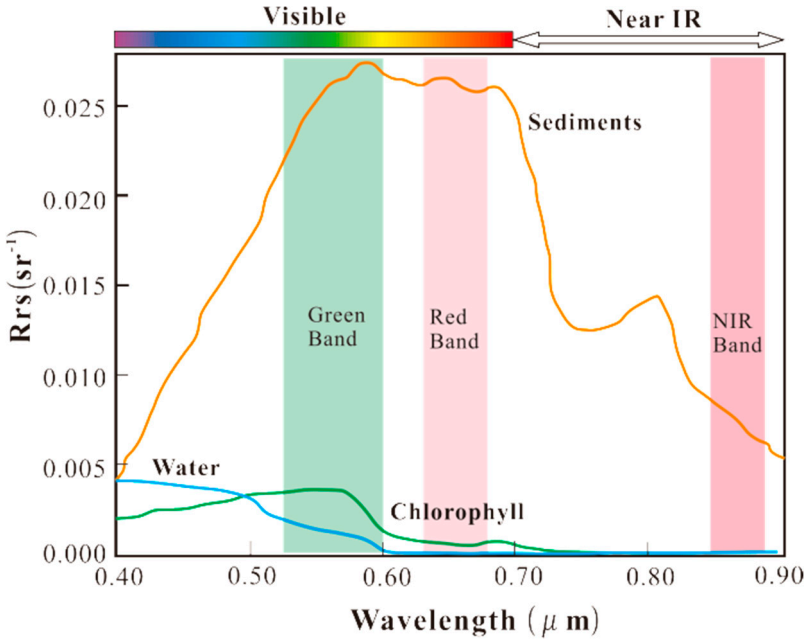

Figure 5. Remote sensing reflectance (Rrs) of clear water (blue), water with chlorophyll content (green), and water with sediments (orange). The green, red, and NIR bands of Landsat 8 images are drawn in the above figure. Note that the figure is modified from Sherry's research [44].

3.2.3. Suspended Sediment Detection

Remote sensing techniques have been widely used to measure qualitative parameters of water bodies [45], including turbidity [46], chlorophyll-a [47], Colored Dissolved Organic

matters (CDOM) [48], Secchi disk depth [49], and water temperature [50]. Here, the concentration of suspended sediment is chosen to examine the degree of waste pollution of Paraopeba River after the Brumadinho dam disaster. The suspended sediment is one of the most important water quality parameters, which directly affects the optical properties of water, such as transparency, turbidity, watercolor, and aquatic ecological conditions [51]. In particular, the level of water turbidity is dependent on the concentration of suspended sediment in the water body. With the increase of suspended particles, it is more difficult for light to travel through the water, and as a result the turbidity of the water increases accordingly. To date, many remote sensing quantitative models have been developed to monitor suspended sediments in water bodies, and several researchers used both the single and double band algorithms to calculate the concentration of suspended sediment of the water body [52–54]. The reflectivity of suspended sediment water is higher in the green and red bands (Figure 5). According to the above band reflectance characteristics, Wang et al. [55] proposed the concept of sediment index as follows:

$$SI = (Green + Red)/(Green/Red) \quad (2)$$

where SI is the sediment parameter, Green and Red are the reflectance in green and red bands, corresponding to 30 m resolution bands 3 and 4 of the Landsat 8 OLI image. Compared with the field-measured data, the correlation coefficient between the measured data and SI value is 0.89 [55], which shows that this method can directly and quantitatively reflect the relative concentration distribution of suspended sediments. The following indicators (Table 2) were used as the criteria to divide different suspended sediment water bodies (M represents the average, D represents the standard deviation, and MIN represents the minimum value):

Table 2. Level of sediment concentration in water bodies.

Indicator Criteria	Level of Sediment Concentration
$SI > M + D$	High suspended sediments
$M < SI \leq M + D$	Medium suspended sediments
$M - D < SI \leq M$	Low suspended sediments
$MIN < SI \leq M - D$	Clean water

3.2.4. Spatiotemporal Pattern Mining

Spatiotemporal pattern mining is often used to analyze data distribution and patterns in space and time. The emerging spatiotemporal hot spot analysis regards data cubes as input and identifies statistically significant hot and cold point trends over time. Using this method, the spatiotemporal hot spots of tailings dam failure database were analyzed. In this study, five main hot spots including New Hot Spot, Consecutive Hot Spot, Sporadic Hot Spot, Oscillating Hot Spot, and No Pattern were detected. Their definitions are listed in Table 3.

3.3. Technical Route

In order to make the structure of the article clearer, the technical route is shown in Figure 6. In this study, we made full use of the available remote sensing images to examine the Brumadinho tailings dam failure disaster. Firstly, we collected different remote sensing data from different data sources. Secondly, we used the true color remote sensing images from NASA to investigate the hazard chain along the gully where the dam failure occurred. Thirdly, considering that the river width is narrow and the medium resolution remote sensing image cannot meet the needs, we used the multi-temporal high-resolution remote sensing images from Google Earth to interpret the transport process of waste along the Paraopeba River. Fourthly, we used the original Landsat 8 images to carry out the analysis of waste diffusion in the reservoirs. Through the above procedure, the whole disaster process was clearly recovered using RS techniques. Last but not least, we used

the global tailings dam failures database to examine tailings-dam-failure trends based on spatiotemporal pattern mining, and found that this area where the Brumadinho tailings dam failure occurred belonged to the Consecutive Hot Spot area with a relatively high risk.

Table 3. Definitions of different hot spots [56].

Name	Meaning
New Hot Spot	A location that is a statistically significant hot spot for the final time step, and has never been a statistically significant hot spot before.
Consecutive Hot Spot	A location that is a single uninterrupted run of statistically significant hot spot in the final time-step intervals.
Sporadic Hot Spot	A location that is an on-again then off-again hot spot.
Oscillating Hot Spot	A location that is a statistically significant hot spot for the final time-step interval with a history of also being a statistically significant cold spot during a prior time step.
No Pattern Detected	A location that does not fall into any of the hot or cold spot patterns defined above.

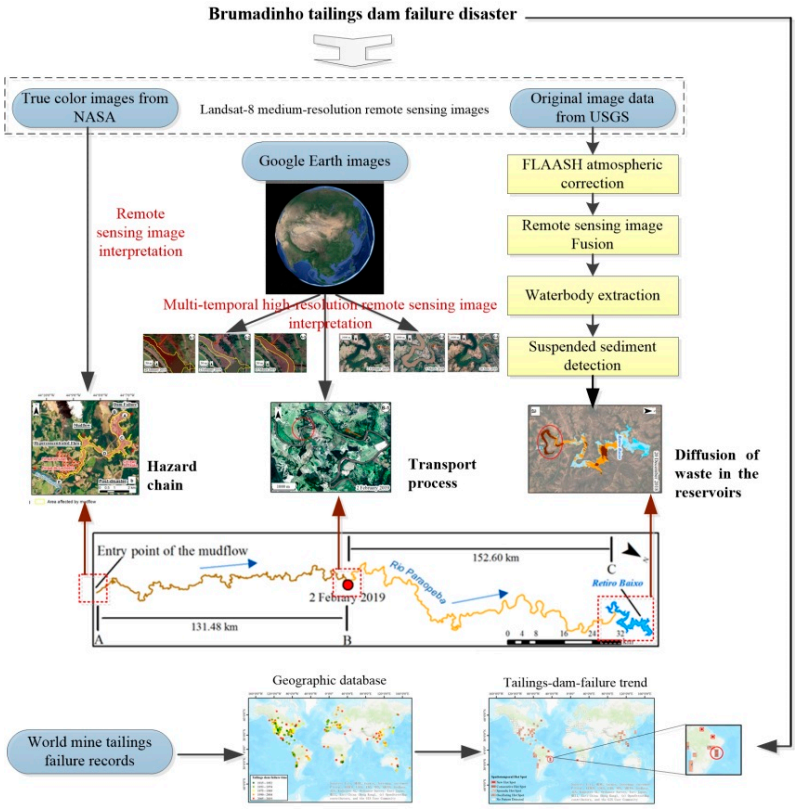

Figure 6. Technical route.

4. Results

4.1. Hazard Chain Caused by This Event

Hazard chains are the hot topic in the broader realm of natural hazards [57] (e.g., earthquake-induced chains [58], glacial-outburst-induced chains [59], and volcano-eruption-induced chains [60]). In this disaster, the dam released a mudflow of tailings after the dam failure (Figure 7b-A). The high-speed mudflow struck the mine's administrative area (Figure 7b-C) [61], destroyed the railway bridge (Figure 3b,c and Figure 7b-D), and continued to move downstream. At about 3:50 pm on 25 January 2019, the mud reached and came into the Paraopeba River (Figure 7b-E). On 27 January 2019, around 5:30 am, sirens

were sounded for the stability of the mine's adjacent Dam VI [16] (Figure 7b-B), where increased water levels were observed.

This hazard chain contained three stages including dam failure, mudflow, and hyperconcentrated flow with tailings waste (Figure 7b). The occurrence of this hazard chain is the result of a combination of many factors. Since the tailings contained a certain amount of water, it created conditions for the mudflow after the tailings dam failure. The tailings waste entered the river following the original branch channel, which in turn enlarged the impact of this disaster with extremely high turbidity and metal concentrations, lower dissolved oxygen, and change of microbial communities which would impact the growth and reproduction of aquatic creatures [62,63].

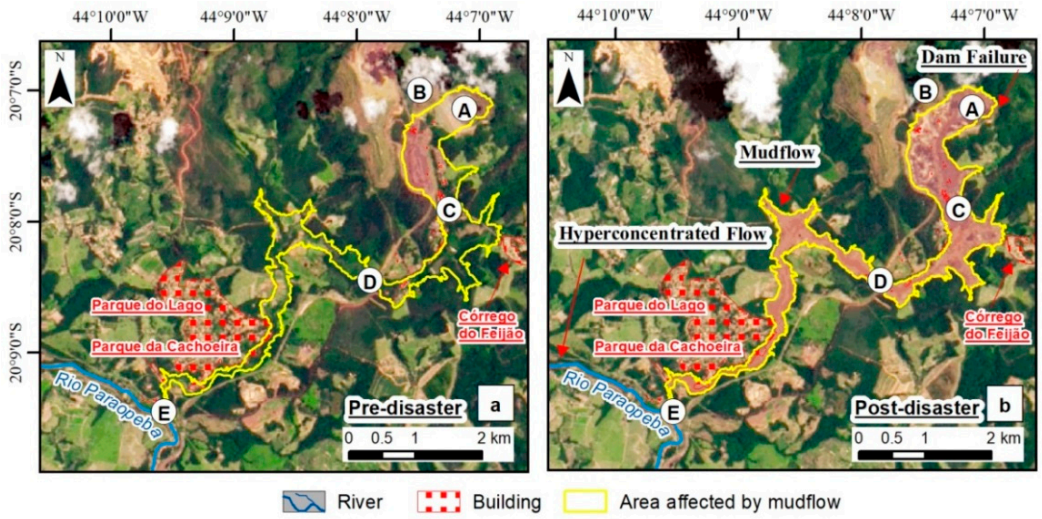

Figure 7. Comparison of pre- and post-disaster Landsat 8 images [64]. (**a**) Pre-disaster remote sensing image (14 January 2019) [27]; (**b**) post-disaster remote sensing image (30 January 2019) [28]. A = location of the destroyed tailings dam and the tailings pond "Barragem I" on 25 January 2019. B = location of tailings pond "Barragem VI" which appeared as an early warning of stability on 27 January 2019. C = location of the destroyed cantina and office buildings. D = location of the destroyed railway bridge (Figure 3b,c). E = location of the entry point of the mudflow into the Paraopeba River.

4.2. Transport Process of Waste in the Rio Paraopeba River

Through the examination of multi-temporal Google Earth images, the transport process of waste in the Paraopeba River can be observed (Figure 8). Comparing Figure 8A-1 with 8A-2, a large amount of waste entered the river several days after the failure, which might block the river for a certain period. Figure 8A-3 shows that due to the increase of precipitation in the later period (Figure 13), the water level of the river increased and eroded a new channel.

Figure 8B-1 shows the location of the waste as of 2 February 2019. It can be observed that the color of the right river section is vermeil, compared with the left section (red circle). The length of AB reach is 131.48 km with a height difference of about 60 m. It took less than a week for the waste to transport from A to B. After the waste entered the Paraopeba River, the transport speed of waste in the water was affected by many factors, such as concentration and stream gradients [65,66]. In addition, according to remote sensing images of Google Earth, it appears that the barrier of some small river dams in the Paraopeba River might also slow down the movement of the waste. Figure 8B-1 is a true-color image of tailings in rivers, and the change of water color in the circle position can be observed. In order to make the watercolor contrast more obvious, considering that the green and red bands are sensitive to the sediment [67], the ratio between these bands were calculated. As can be seen in Figure 8B-2, there is an obvious change in water color at the red circle.

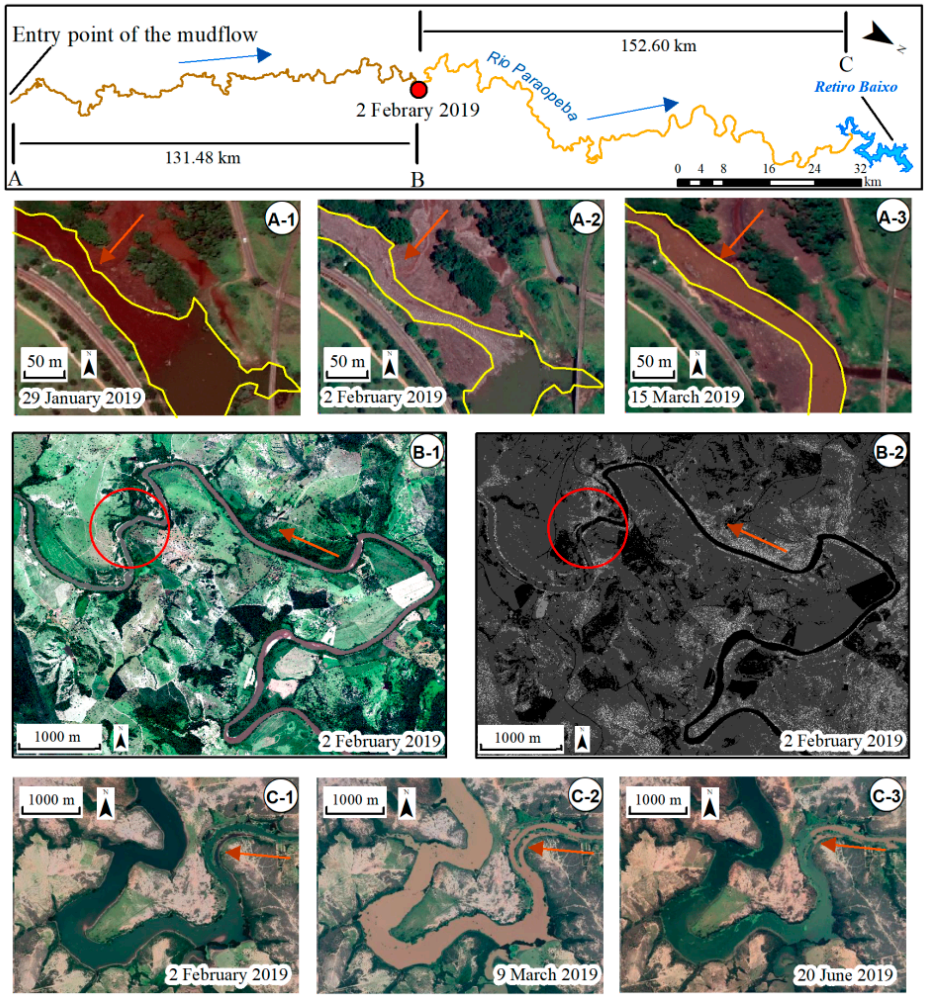

Figure 8. Transport process of waste in the Paraopeba River. A—1, 2, 3 = images of the entry point of the mudflow into the Paraopeba River, the yellow lines are used to mark the river boundary; B—1, 2 = images on 2 February 2019 around point B in the Paraopeba River, the watercolor change can be seen; C—1, 2, 3 = images of the entry point into the Retiro Baixo.

Comparing Figure 8C-1 with 8C-2, the influence of waste on the water body was obvious after it entered the reservoir of hydropower station—Retiro Baixo. A few months later, the watercolor recovered due to the deposition of sediments. Based on the analysis of Figure 8 and multi-temporal Google Earth images, a table of sediment transport time node was generated (Table 4) in order to make the interpretation of sediment transport clear.

Table 4. Sediment transport time nodes.

Locations	Dates					
	25 January	29 January	2 February	9 March	15 March	20 June
A		A-1	A-2		A-3	Unknown
B			B-1 and B-2			
C			C-1	C-2		C-3

Note: The brown color indicates that the location exhibits sediments on that specific date, while the blue color implies that there was no sediment transported to this location or sediments had settled down.

4.3. Diffusion of Waste in the Reservoirs of Two Hydroelectric Plants

(1) Determination of reservoir boundaries

Using the Atmospheric Correction Module, it can be accurately compensated for atmospheric effects. In this study, the atmospheric correction using the FLAASH model [34,35,68] was performed and Landsat 8 images were fused using the Gram—Schmidt Pan Sharpening method [69–72]. After calculating the NDWI using the images after atmospheric correction and image fusion, zero was used as the segmentation threshold to extract the water body, and the manual editing was used to complete the extracted water body boundaries in the ArcGIS software. Figure 9 shows the boundaries of two reservoirs, Retiro Baixo and Três Marias.

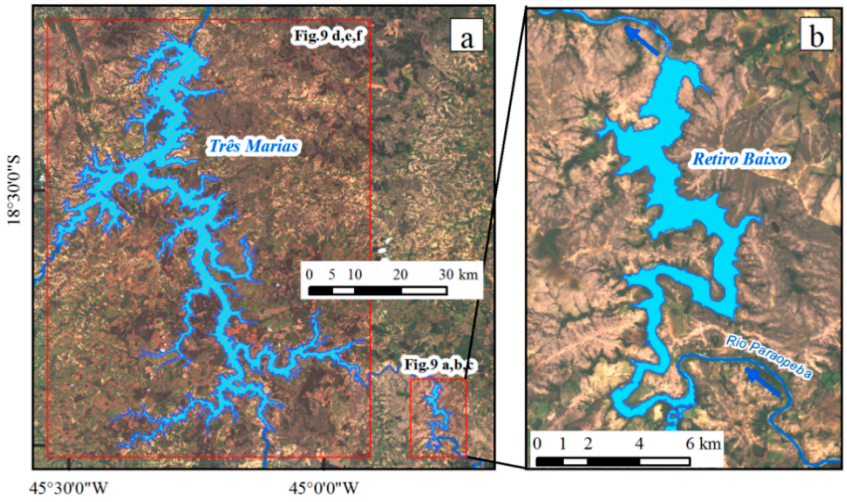

Figure 9. (**a**) Retiro Baixo and Três Marias reservoirs. The larger reservoir on the left is Três Marias, and the smaller one in the lower right corner is Retiro Baixo (**b**).

(2) Sediment index used to estimate the level of sediment concentration

The sediment index was obtained using the SI calculating method. Figure 10 shows the pre- and post-disaster sediment concentrations. Contrasting the area of high sediment concentration where the river enters into the Retiro Baixo reservoir (Figure 10a–c), it had a larger area of 3.66 km^2 compared with 1.89 km^2 on 20 December 2018 and 2.49 km^2 on 27 April 2019 with a 2-month interval spanning this disaster. It can be observed that the sediment plume had a great impact on the reservoir of the Retiro Baixo Plant, over 300 km from the failure location, while less impact on the reservoir of the Retiro Baixo Plant. This result is consistent with Vale's evaluation [73]. It appeared that small river gradients and obstruction of the reservoir barriers played an important role in slowing down the tailings waste moving into the São Francisco River. It is not hard to find out that this disaster event had little impact on the Três Marias reservoir (Figure 10d–f).

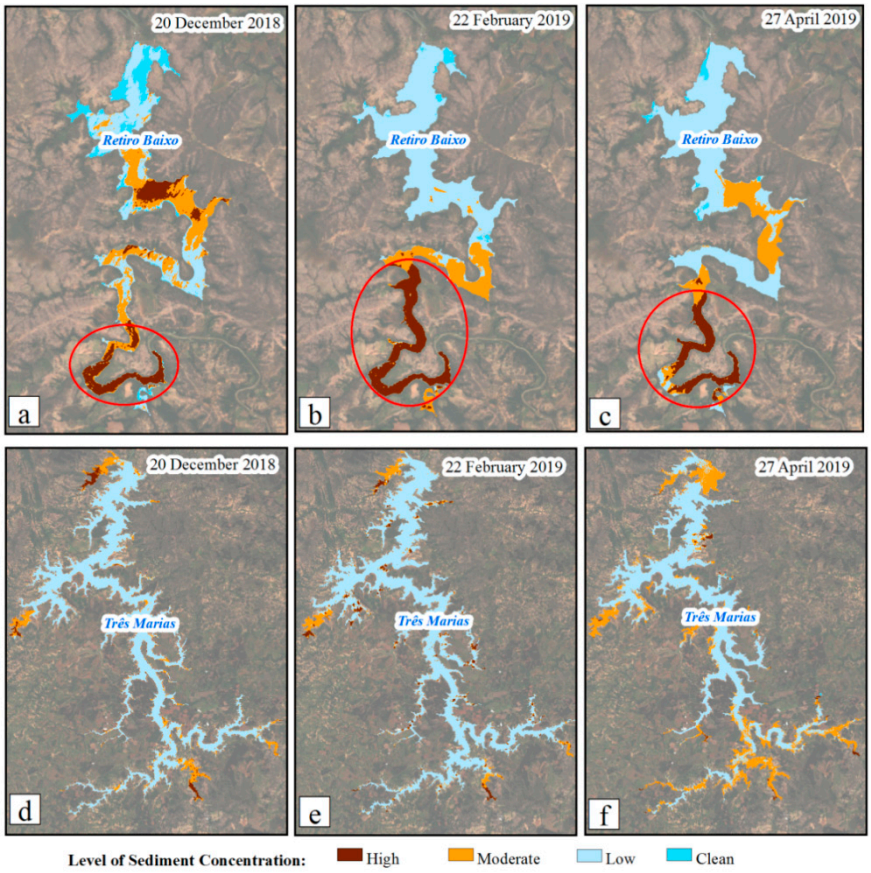

Figure 10. Level of sediment concentration of Retiro Baixo and Três Marias. (**a**) Level of sediment concentration of Retiro Baixo on 20 December 2018; (**b**) level of sediment concentration of Retiro Baixo on 22 February 2019; (**c**) level of sediment concentration of Retiro Baixo on 27 April 2019; (**d**) level of sediment concentration of Três Marias on 20 December 2018; (**e**) level of sediment concentration of Três Marias on 22 February 2019; (**f**) level of sediment concentration of Três Marias on 27 April 2019.

4.4. Tailings-Dam-Failure Trend Analysis Based on Spatiotemporal Pattern Mining

Using the emerging spatiotemporal hot spot analysis method, it can be found that the Brumadinho dam disaster in Brazil belongs to the Consecutive Hot Spot area (Figure 11). This disaster happened 3 years and 2 months after the Mariana dam disaster (5 November 2015), which was considered the worst environmental disaster in Brazil [74,75]. The Brumadinho and Mariana dam disasters both occurred in Minas Gerais, Brazil, and the two dams were both owned by Vale, a Brazilian multinational corporation engaged in metals and mining. Furthermore, based on the world mine tailings failure records [14], tailings dam failures have been recorded several times in this area. As a result, this area belongs to the Consecutive Hot Spot area, and the risk of tailings dam failure in this area would be relatively high if the necessary pond's management and the engineering safety measures were not carried out.

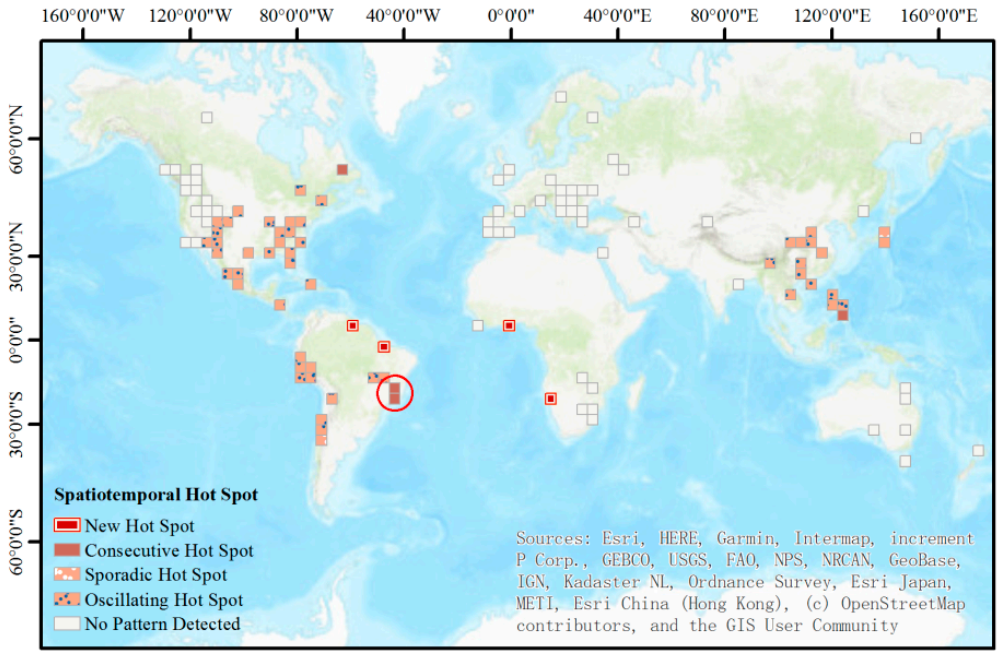

Figure 11. Spatiotemporal hot spot analysis of tailings dam failures. The location of Brumadinho dam disaster is marked with red circles.

According to Figure 11, New Hot Spots appear in Africa and South America which belong to developing regions, where the mining industry has been an important economic pillar in recent years [76,77]. Consecutive Hot Spots mainly lie in Eastern South America and Western Pacific islands where there are a lot of tailings left by mining, but due to poor management, tailings failure is easy to occur. The Sporadic Hot Spot is in Southwest South America and Oscillating Hot Spots mainly lie in Asia and America. China has many Oscillating Hot Spots and there have been some particularly serious tailings failure disasters, such as the 8 September 2008 dam break accident in Shanxi [78]. Different hot spots have different characteristics of disaster occurrences. These characteristics can be influenced by the mining history, mining features (e.g., man-made or natural), etc. [79–81]. The recommendation is that different hot spots should be treated differently. The areas of New Hot Spots and Consecutive Hot Spots are the ones that deserve the most attention. Local governments should adopt appropriate risk management strategies to monitor and change the trend. The risk assessment and monitoring of tailings reservoirs should be adopted and implemented. In this regard, some risk assessment and monitoring methods of mountain disasters can be used as references [82–85].

5. Discussion

5.1. Cause Analysis of This Disaster

5.1.1. Lack of Stability Management during the Maintenance Stage

Some experts believed that Brazil's weak regulatory structures and regulatory gaps allowed the dam's failure [86]. This dam was built in 1976 using the "upstream" method, in which coarse rubble, compacted soil, and dried tailings were used to build the dam (Figure 12). This is similar to the Fundão dam which failed in November 2015, killing 19 people and causing an environmental catastrophe, compared with a more expensive and strong method using solid rocks to contain the waste. The water leak was first observed near its base in July 2018, and then repairs were carried out [87]. José de Gouveia, the worker of Vale, said that the dam exhibited a small leak soon after the rainy season, and leaking water was observed in several places at the bottom [87]. The possible pore pressure build-up would have resulted in a decrease in effective stress and initiated a failure.

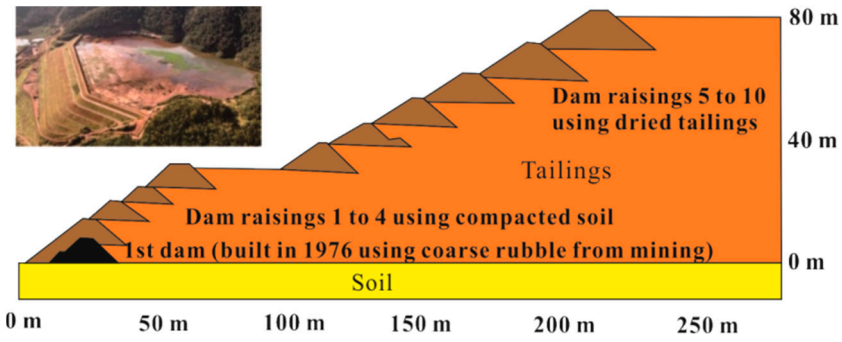

Figure 12. Cross section of Brumadinho dam "Barragem I" from the west to the east [88,89].

5.1.2. Extreme Weather Effects

In this section, weather effects are examined. Daily precipitation data in Brumadinho were obtained from the World Weather Online website [90]. It appeared that precipitation increased the water content of the tailings pond before the dam failure event, increased the pore pressure, and thus induced failure initiation, which could be an important triggering factor for the tailings dam collapse (Figure 13). Although there was less rainfall in January than in February and March 2019, the rainfall in January 2019 sometimes reached the peak of monthly rainfall in some years from the perspective of multi-year rainfalls (Figure 14).

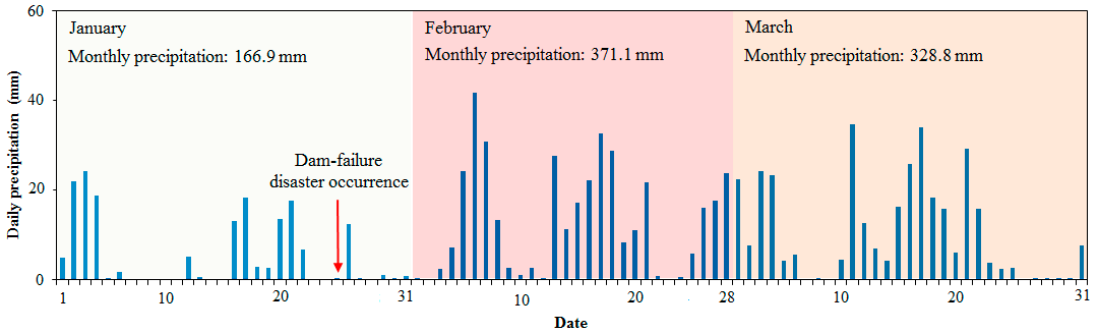

Figure 13. Daily precipitation in Brumadinho during the period from January to March 2019 [90].

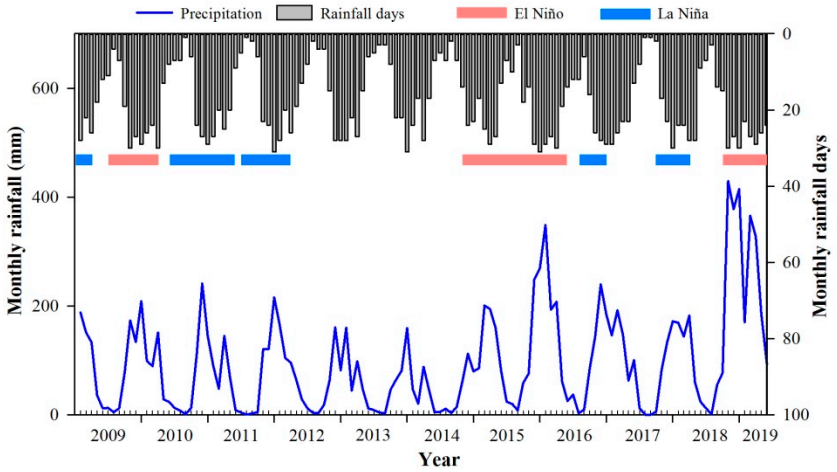

Figure 14. Monthly precipitation in Brumadinho during the period from 2009 to 2019 [90].

El Niño and La Niña events are complex weather patterns resulting from variations in ocean temperatures in the Equatorial Pacific [91]. Their circulation is a global scale climate oscillation. Generally, the impacts of most El Niño events include above-average rainfalls in southeastern South America, eastern equatorial Africa, and the southern USA [92].

Extreme weathers in Brumadinho are linked to El Niño conditions from September to January typically [93]. A major El Niño event has been recorded since October 2018, and there were unusual rainfalls before the disaster (Figure 14) [94]. The increase of soil water content created conditions for the dam instability.

5.2. Lessons Learned and Perceptions about Safety Management of Tailings Ponds

The catastrophic tailings dam failure disaster that occurred in Brumadinho, Brazil is worthy of reviewing the safety management of tailings ponds in order to reduce the occurrence of such incidents. Tailings pond management has the characteristics of a heavy task and wide involvement, and requires the cooperation of different departments and joint law enforcement. The participation of multiple departments also illustrates that tailings pond management is a comprehensive and complex task involving disaster, development, industry, finance and taxation, resources, ecology, water conservancy, meteorology, and other fields [95–97]. At the same time, the successful completion of this task requires interdisciplinary integration and close cooperation of the related fields. Based on the above considerations, the following recommendations are made as a reference:

(1) **Set up a joint working group for tailings pond management, and build a unified management platform, in order to guide tailings pond management**. The comprehensive management work of tailings ponds involves many departments and disciplines. Relevant personnel should be selected from each department for the docking of the management work, and a joint working group should be established to actively and steadily promote the management work of tailings ponds. In addition, according to the needs of governance work, researchers from relevant disciplines of scientific research institutes and universities should be invited to join the joint working group as consulting experts to carry out academic exchanges. Through multidisciplinary exchanges and interdisciplinary integration, theoretical support and technical support could be provided for tailings pond management [98].

(2) **Build the basic geographic information database of tailings ponds, and obtain the basic data of tailings ponds.** The geographic database is an effective way to scientifically organize and manage geographic data. To find out the stock and spatial distribution of tailings ponds is the premise to realize the comprehensive and efficient management of tailings ponds in the later period. During the treatment period of tailings ponds, the number of tailings ponds fluctuates greatly, and some of the abandoned tailings ponds with a long history and a small size may cause statistical omissions. Therefore, it is urgent to find out the basic data of tailings ponds through a detailed investigation and real-time dynamic update and adjustment. Based on the above problems, remote sensing image interpretation [99], literatures and field investigation [100], telephone polls, etc. could be used to obtain the location of the tailings pond, year of construction, condition of use, storage of the pond, height of the tailings dam, type of tailings, and the geographic database could be used for the unified organization and management of the above date [101]. Later, a new investigation information could be used to dynamically update the database.

(3) **The sites selection of new tailings ponds should take into consideration many factors such as safety, ecology, sustainability, and land planning, so as to realize "whole-chain" planning and guide the whole life cycle of tailings ponds with a system engineering theory** [102,103]. A complete life cycle of the tailings pond should start from site selection, go through the process of construction, operation and management, and finally take "reduction" as the end of the mission of a tailings pond. Therefore, the problems needed to be considered in the planning stage of the new tailings ponds include: First, whether geological, geomorphic, environmental, and other factors are suitable for the construction of tailings ponds [104]; second, whether the tailing dams could meet the relevant standards and requirements [105]; third, how to monitor and simulate the stability in the running stage of the tailings pond [106,107]; fourth, how to carry out the comprehensive treatment after the tailings

pond is stopped, the follow-up treatment of tailings, the ecological restoration, and land use planning of the mining area after the tailings treatment [108,109]. The above plans finally form a "whole chain" plan, and the system engineering theory would be introduced into it. On the basis of interdisciplinary integration, the overall optimal operation of the tailings pond system could guide the entire life cycle of the tailings pond. During the management of tailings ponds, the problem of tailing pond failures is the most important part. Such failures are mainly related to geotechnical engineering. Engineering measures should be taken to evaluate and control the water content in the reservoir and pore water pressure. To evaluate the slope stability a range of geotechnical datasets are necessary, including tailing granulometry, hydraulic conductivity, effective porosity, water level in the pond, and pore pressure under meteorological stresses. Based on these datasets, hydraulic simulations, followed by slope stability simulations will lead to the establishment of design requirements.

(4) **Integrate multi-discipline to carry out the comprehensive safety assessment of the built tailings ponds, make clear the management sequence of tailings ponds**. The safety of the tailings pond and its impact on the ecological environment are the two most concerned issues of the built tailings pond. Therefore, it is necessary to organize engineering researchers to evaluate the stability of the built tailings pond and complete the safety risk and ecological risk assessment of the tailings pond together with ecological researchers [110,111]. Comprehensively considering safety risks and ecological risks, priority treatment objects for the tailings pond treatment could be selected in order to improve the utilization efficiency of governance funds [112]. Some engineering measures to improve the stability of the tailing ponds are necessary, such as gentle slopes, norms regarding the maximum height of dams, drainage systems and simulation of their influence on the slope stability, mathematical simulations to evaluate the slope stability under different meteorological conditions, projects for closing the ponds, etc.

(5) **The study on efficient utilization of tailings ponds should be carried out in order to clarify the concept that "tailings are the resource in the wrong place".** The definition of tailing indicates that tailing is the part with a too low content of the target component to be used in production. With the progress of science and technology and the improvement of the efficient utilization ability of mineral resources, on the one hand, the target components in the tailings pond have the possibility of being re-extracted and utilized. On the other hand, other components in the tailings may become effective components in other industries and could be utilized. Nowadays, tailings reuse has made great progress in many aspects, such as heavy separation of useful materials, production of building materials, production of fertilizers, and filling of mine goaf [113–115]. The efficient utilization of tailings ponds in the later stage needs further research and new technology support, but the cognition of tailings from "waste" to "resource" also needs to be changed.

(6) **Mine tailings reservoir potential tourism value, broaden the tourism resources of industrial heritage.** Tailings ponds are the product of the industrial age, but also the unique brand of the industrial age, with obvious characteristics. Tailings ponds and their surrounding mining industry remains constitute an organism of history, technology, society, architecture, and industrial heritage with a scientific value. The organism becomes a witness of history, and has become one of the important tourism contents today [116,117]. After transforming, industrial sites can be transformed into beneficial scenic spots with the function of education. There is a long way for the transformation of industrial heritages into successful tourism products, but there have been many successful cases to learn from, such as Ruhr area in Germany [118] and Beijing 798 Art Zone [119]. The development of industrial heritage tourism resources of tailings ponds needs the full cooperation of scholars such as planning, tourism, and heritage protection, and also needs the strong support of government departments.

6. Conclusions

Tailings reservoir materials are easy to cause harm to the environment, and dam-failure disasters often occur in production mining areas where there are population and production equipment. Therefore, the damages caused by such disasters are often more serious than others, and more attention should be paid. In this study, we carried out a disaster investigation of the Brumadinho tailings failure event. A detailed analysis of the Brumadinho tailing dam failure disaster was carried out using medium to high-resolution satellite images covering the entire affected areas of the event, including the place where the disaster occurred to the transport of tailings in the river and its impact on downstream reservoirs. Especially, the research of the diffusion of sediment in the reservoir was done in order to assess the impact of tailing waste, and discuss whether the waste reached the dams of two hydroelectric plants: Retiro Baixo and Três Marias or even the São Francisco River. Different from those caused by common landslides and debris flows, the disasters caused by the tailings dam failure are more serious and could affect larger areas due to the tailing waste pollution, and they should be paid more attention. On the other hand, the impacts of climatic factors on this event were also discussed in order to make people pay attention to the relationship between extreme weather events and nature disasters. Most importantly, the temporal and spatial characteristics of tailings dam failure were analyzed and summarized by building a global tailings dam failure database. The following conclusions are drawn:

1. The analysis of disaster characteristics revealed that the Brumadinho disaster could be identified as a hazard chain caused by dam failure, mudflow, and hyperconcentrated flow. Especially, the tailings made a great impact on the reservoir of the Retiro Baixo Plant.
2. The Brumadinho disaster is the result of weak regulatory structures and regulatory gaps. However, the influence of weather factors cannot be ignored.
3. The in-depth analysis and interpretation of rainfall data over 11 years revealed that the El Niño event which started in 2018 increased the rainfall, and in turn played an important role and affected the stability of tailings soil.
4. Based on the spatiotemporal analysis of the global tailings dam failure disaster events, different types of hot spots were found. Different hot spots should be dealt with different coping strategies.
5. This disaster also shows that the risk assessment, monitoring, and early warning of tailings ponds in mining areas are necessary for disaster prevention and mitigation.

Author Contributions: Conceptualization, Y.C.; methodology, D.C. and Y.C.; formal analysis, D.C.; supervision, Y.C.; validation, Y.C. and Z.L.; writing—original draft, D.C. and Y.C.; writing—review and editing, Z.L. and J.I.; funding acquisition, Z.L. and Y.C. All authors have read and agreed to the published version of the manuscript.

Funding: This research was funded by the National Natural Science Foundation of China (reference numbers 41941019 and 42077238), and the Chinese Academy of Sciences through the International partnership program (reference number 131551KYSB20160002). Part of this work was also supported by the Shaanxi Province Science and Technology Innovation team (reference number 2021TD-51), the Fundamental Research Funds for the Central Universities, CHD (reference numbers 300102260301 and 300102261108), and by the European Space Agency through the ESA-MOST DRAGON-5 project (reference number 59339). The authors are grateful for the Key Research Program of Frontier Sciences, CAS (grant number QYZDY-SSW-DQC006), and the Chinese Academy of Sciences President's International Fellowship Initiative (grant number 2021VCB0003).

Data Availability Statement: Our research data are from relevant open data websites, which can be obtained according to the links listed in our references.

Acknowledgments: The authors would like to thank all colleagues who participated in this study.

Conflicts of Interest: The authors declare no conflict of interest.

References

1. Rico, M.; Benito, G.; Salgueiro, A.R.; Diez-Herrero, A.; Pereira, H.G. Reported tailings dam failures. A review of the European incidents in the worldwide context. *J. Hazard. Mater.* **2008**, *152*, 846–852. [CrossRef] [PubMed]
2. Franks, D.M.; Boger, D.V.; Côte, C.M.; Mulligan, D.R. Sustainable development principles for the disposal of mining and mineral processing wastes. *Resour. Policy* **2011**, *36*, 114–122. [CrossRef]
3. Macklin, M.G.; Brewer, P.A.; Balteanu, D.; Coulthard, T.J.; Driga, B.; Howard, A.J.; Zaharia, S. The long term fate and environmental significance of contaminant metals released by the January and March 2000 mining tailings dam failures in Maramureş County, upper Tisa Basin, Romania. *Appl. Geochem.* **2003**, *18*, 241–257. [CrossRef]
4. Porsani, J.L.; Jesus, F.A.N.d.; Stangari, M.C. GPR survey on an iron mining area after the collapse of the tailings dam I at the Córrego do Feijão Mine in Brumadinho-MG, Brazil. *Remote Sens.* **2019**, *11*, 860. [CrossRef]
5. Yu, D.; Tang, L.; Chen, C. Three-dimensional numerical simulation of mud flow from a tailings dam failure across complex terrain. *Nat. Hazards Earth Syst. Sci.* **2020**, *20*, 727–741. [CrossRef]
6. Mizani, S.; He, X.; Simms, P. Application of lubrication theory to modeling stack geometry of high density mine tailings. *J. Non Newton. Fluid Mech.* **2013**, *198*, 59–70. [CrossRef]
7. Al-Husseinawi, Y.; Li, Z.; Clarke, P.; Edwards, S. Evaluation of the stability of the Darbandikhan Dam after the 12 November 2017 Mw 7.3 Sarpol-e Zahab (Iran–Iraq border) earthquake. *Remote Sens.* **2018**, *10*, 1426. [CrossRef]
8. Cheng, D.; Cui, Y.; Su, F.; Jia, Y.; Choi, C.E. The characteristics of the Mocoa compound disaster event, Colombia. *Landslides* **2018**, *15*, 1223–1232. [CrossRef]
9. Cui, Y.; Cheng, D.; Choi, C.E.; Jin, W.; Lei, Y.; Kargel, J.S. The cost of rapid and haphazard urbanization: Lessons learned from the Freetown landslide disaster. *Landslides* **2019**, *16*, 1167–1176. [CrossRef]
10. Metternicht, G.; Hurni, L.; Gogu, R. Remote sensing of landslides: An analysis of the potential contribution to geo-spatial systems for hazard assessment in mountainous environments. *Remote Sens. Environ.* **2005**, *98*, 284–303. [CrossRef]
11. Silveira, E.M.d.O.; Júnior, F.W.A.; Mello, J.M.d.; Bueno, I.T. Object-based change detection using semivariogram indices derived from NDVI images: The environmental disaster in Mariana, Brazil. *Ciência e Agrotecnologia* **2017**, *41*, 554–564. [CrossRef]
12. Grenerczy, G.; Wegmüller, U. Persistent scatterer interferometry analysis of the embankment failure of a red mud reservoir using ENVISAT ASAR data. *Nat. Hazards* **2011**, *59*, 1047–1053. [CrossRef]
13. Schvartsman-F. Fabio Schvartsman—Annoucement about Brumadinho Breach Dam. Available online: http://www.vale.com/brasil/EN/aboutvale/news/Pages/fabio-schvartsman-annoucement-about-brumadinho-breach-dam.aspx (accessed on 17 August 2019).
14. WMTF. World Mine Tailings Failures—From 1915. Available online: https://worldminetailingsfailures.org/ (accessed on 17 August 2019).
15. G1. Tragédia em Brumadinho: Lista da Vale de Pessoas não Encontradas. Available online: https://g1.globo.com/mg/minas-gerais/noticia/2019/01/26/vale-divulga-lista-de-pessoas-sem-contato-em-brumadinho.ghtml (accessed on 17 August 2019).
16. Sky-news. Brazil Dam Rescue Resumes after Second Barrier Ruled Safe. Available online: https://news.sky.com/story/brazil-dam-collapse-imminent-risk-of-further-rupture-sparks-evacuation-11619213 (accessed on 17 August 2019).
17. World-Animal-Protection. Helping Animals after Brazil Dam Collapse. Available online: https://www.worldanimalprotection.ca/news/helping-animals-after-brazil-dam-collapse (accessed on 17 August 2019).
18. Lempriere, M. Time to Talk about Tailings Dams. Available online: https://www.mining-technology.com/features/time-to-talk-about-tailings-dams/ (accessed on 17 August 2019).
19. Ibama. Brumadinho, Minas Gerais. Available online: https://commons.wikimedia.org/w/index.php?curid=76936072 (accessed on 17 August 2019).
20. TV-NBR. Resumo da Agenda do Presidente da República 26.01.2019 (Video Screenshot) 01. Available online: https://pt.wikipedia.org/wiki/Ficheiro:Resumo_da_agenda_do_Presidente_da_Rep%C3%BAblica_26.01.2019_(video_screenshot)_01_(cropped).png (accessed on 17 August 2019).
21. Venaglia, G. Iron Ore Railway Bridge Destroyed by Mudflow, 3 Kilometres (1.9 mi) Downstream from Collapsed Dam. Available online: https://en.wikipedia.org/wiki/Brumadinho_dam_disaster#/media/File:Brumadinho4.jpg (accessed on 17 August 2019).
22. Gao, K.; Cui, P.; Zhao, C.; Wei, F. Landslide hazard evaluation of Wanzhou based on GIS information value method in the Three Gorges Reservoir. *Yanshilixue Yu Gongcheng Xuebao Chin. J. Rock Mech. Eng.* **2006**, *25*, 991–996.
23. Cui, Y.; Cheng, D.; Chan, D. Investigation of Post-Fire Debris Flows in Montecito. *ISPRS Int. J. Geo Inf.* **2019**, *8*, 5. [CrossRef]
24. Malarvizhi, K.; Kumar, S.V.; Porchelvan, P. Use of high resolution Google Earth satellite imagery in landuse map preparation for urban related applications. *Procedia Technol.* **2016**, *24*, 1835–1842. [CrossRef]
25. Rabby, Y.W.; Li, Y. An integrated approach to map landslides in Chittagong Hilly Areas, Bangladesh, using Google Earth and field mapping. *Landslides* **2018**, *16*, 633–645. [CrossRef]
26. Cheng, D.; Gao, C.; Shao, T.; Iqbal, J. A landscape study of Sichuan University (Wangjiang Campus) from the perspective of campus tourism. *Land* **2020**, *9*, 499. [CrossRef]
27. NASA-Earth-Observatory. Another Deadly Dam Collapse in Brazil 01.Jpg. Available online: https://commons.wikimedia.org/wiki/File:Another_Deadly_Dam_Collapse_in_Brazil_01.jpg (accessed on 10 August 2019).
28. NASA-Earth-Observatory. Another Deadly Dam Collapse in Brazil 02.Jpg. Available online: https://commons.wikimedia.org/wiki/File:Another_Deadly_Dam_Collapse_in_Brazil_02.jpg (accessed on 10 August 2019).

29. USGS. Glovis. Available online: https://glovis.usgs.gov/ (accessed on 17 August 2019).
30. Edumine. Advance Your Career. Available online: http://www.infomine.com/publications/docs/Martin2000.pdf (accessed on 17 August 2019).
31. UN-Environment. Dam or be Damned: Mining Safety under Scrutiny. Available online: https://www.unenvironment.org/news-and-stories/story/dam-or-be-damned-mining-safety-under-scrutiny (accessed on 17 August 2019).
32. Martins, V.S.; Barbosa, C.C.F.; De Carvalho, L.A.S.; Jorge, D.S.F.; Lobo, F.D.L.; Novo, E.M.L.d.M. Assessment of atmospheric correction methods for Sentinel-2 MSI images applied to Amazon floodplain lakes. *Remote Sens.* **2017**, *9*, 322. [CrossRef]
33. ENVI. Atmospheric Correction Module: QUAC and FLAASH User's Guide. Available online: http://www.exelisvis.com/portals/0/pdfs/envi/Flaash_Module.pdf (accessed on 11 July 2019).
34. Guo, Y.; Zeng, F. Atmospheric correction comparison of SPOT-5 image based on model FLAASH and model QUAC. *Int. Arch. Photogramm. Remote Sens. Spat. Inf. Sci.* **2012**, *39*, 21–23.
35. Vibhute, A.D.; Kale, K.; Dhumal, R.K.; Mehrotra, S. Hyperspectral imaging data atmospheric correction challenges and solutions using QUAC and FLAASH algorithms. In Proceedings of the 2015 International Conference on Man and Machine Interfacing (MAMI), Bhubaneswar, India, 17–19 December 2015; pp. 1–6.
36. Blog ENVI-IDL. Atmospheric Correction of Landsat 8 Data in ENVI5.1. Available online: http://blog.sina.com.cn/s/blog_764b1e9d0101cb2l.html (accessed on 11 July 2019).
37. Nencini, F.; Garzelli, A.; Baronti, S.; Alparone, L. Remote sensing image fusion using the curvelet transform. *Inf. Fusion* **2007**, *8*, 143–156. [CrossRef]
38. Deng, S.; Chen, Q.; Du, H.; Xu, E. *ENVI Remote Sensing Image Processing Method*; Higher Education Press: Beijing, China, 2014; p. 91.
39. Maurer, T. How to pan-sharpen images using the Gram-Schmidt pan-sharpen method—A recipe. *ISPRS Int. Arch. Photogramm. Remote Sens. Spat. Inf. Sci.* **2013**, *239–244*. [CrossRef]
40. Pekel, J.; Vancutsem, C.; Bastin, L.; Clerici, M.; Vanbogaert, E.; Bartholome, E.; Defourny, P. A near real-time water surface detection method based on HSV transformation of MODIS multi-spectral time series data. *Remote Sens. Environ.* **2014**, *140*, 704–716. [CrossRef]
41. Tu, T.; Lee, Y.; Chang, C.; Huang, P.S. Adjustable intensity-hue-saturation and Brovey transform fusion technique for IKONOS/QuickBird imagery. *Opt. Eng.* **2005**, *44*, 116201. [CrossRef]
42. Arenas-Castro, S.; Julien, Y.; Jiménez-Munoz, J.C.; Sobrino, J.A.; Fernández-Haeger, J.; Jordano-Barbudo, D. Mapping wild pear trees (pyrus bourgaeana) in Mediterranean forest using high-resolution QuickBird satellite imagery. *International Journal of Remote Sens.* **2013**, *34*, 3376–3396. [CrossRef]
43. McFeeters, S.K. The use of the Normalized Difference Water Index (NDWI) in the delineation of open water features. *Int. J. Remote Sens.* **2007**, *17*, 1425–1432. [CrossRef]
44. Sherry, L. Fundamentals of Aquatic Remote Sensing. Available online: https://arset.gsfc.nasa.gov/sites/default/files/users/fundamentals/fundamentals-aquatic-web.pdf (accessed on 17 August 2019).
45. Gholizadeh, M.H.; Melesse, A.M.; Reddi, L. A comprehensive review on water quality parameters estimation using remote sensing techniques. *Sensors* **2016**, *16*, 1298. [CrossRef] [PubMed]
46. Wass, P.; Marks, S.; Finch, J.; Leeks, G.J.L.; Ingram, J. Monitoring and preliminary interpretation of in-river turbidity and remote sensed imagery for suspended sediment transport studies in the Humber catchment. *Sci. Total Environ.* **1997**, *194*, 263–283. [CrossRef]
47. Lim, J.; Choi, M. Assessment of water quality based on Landsat 8 operational land imager associated with human activities in Korea. *Environ. Monit. Assess.* **2015**, *187*, 384. [CrossRef]
48. Antoine, D.; d'Ortenzio, F.; Hooker, S.B.; Bécu, G.; Gentili, B.; Tailliez, D.; Scott, A.J. Assessment of uncertainty in the ocean reflectance determined by three satellite ocean color sensors (MERIS, SeaWiFS and MODIS-A) at an offshore site in the Mediterranean Sea (BOUSSOLE project). *J. Geophys. Res. Ocean.* **2008**, *113*. [CrossRef]
49. Lindell, L.; Steinvall, O.; Jonsson, M.; Claesson, T. Mapping of coastal-water turbidity using Landsat imagery. *Int. J. Remote Sens.* **1985**, *6*, 629–642. [CrossRef]
50. Haakstad, M.; Kogeler, J.; Dahle, S. Studies of sea surface temperatures in selected northern Norwegian fjords using Landsat TM data. *Polar Res.* **1994**, *13*, 95–110. [CrossRef]
51. Ryan, P.A. Environmental effects of sediment on New Zealand streams: A review. *N. Z. J. Mar. Freshw. Res.* **1991**, *25*, 207–221. [CrossRef]
52. Doxaran, D.; Froidefond, J.-M.; Lavender, S.; Castaing, P. Spectral signature of highly turbid waters: Application with SPOT data to quantify suspended particulate matter concentrations. *Remote Sens. Environ.* **2002**, *81*, 149–161. [CrossRef]
53. Feng, L.; Hu, C.; Chen, X.; Song, Q. Influence of the Three Gorges Dam on total suspended matters in the Yangtze Estuary and its adjacent coastal waters: Observations from MODIS. *Remote Sens. Environ.* **2014**, *140*, 779–788. [CrossRef]
54. Nechad, B.; Ruddick, K.G.; Park, Y. Calibration and validation of a generic multisensor algorithm for mapping of total suspended matter in turbid waters. *Remote Sens. Environ.* **2010**, *114*, 854–866.
55. Wang, X.; Li, W.; Yan, X.; Lu, Y.; Zhou, X.; Li, X.; Xia, L.; Tang, X.; Mei, C. Information extraction for suspended sediment in Lake Chaohu and its distribution based on Landsat TM/ETM+ data. *J. Lake Sci.* **2007**, *19*, 255–260.

56. Esri. Emerging Hot Spot Analysis. Available online: https://pro.arcgis.com/en/pro-app/tool-reference/space-time-pattern-mining/emerginghotspots.htm (accessed on 17 August 2019).
57. Xu, L.; Meng, X.; Xu, X. Natural hazard chain research in China: A review. *Nat. Hazards* **2013**, *70*, 1631–1659. [CrossRef]
58. Fan, X.; Scaringi, G.; Korup, O.; West, A.J.; Westen, C.J.; Tanyas, H.; Hovius, N.; Hales, T.C.; Jibson, R.W.; Allstadt, K.E.; et al. Earthquake-Induced chains of geologic hazards: Patterns, mechanisms, and impacts. *Rev. Geophys.* **2019**, *57*, 421–503. [CrossRef]
59. Wei, R.; Zeng, Q.; Davies, T.; Yuan, G.; Wang, K.; Xue, X.; Yin, Q. Geohazard cascade and mechanism of large debris flows in Tianmo gully, SE Tibetan Plateau and implications to hazard monitoring. *Eng. Geol.* **2018**, *233*, 172–182. [CrossRef]
60. Walter, T.R.; Haghighi, M.H.; Schneider, F.M.; Coppola, D.; Motagh, M.; Saul, J.; Babeyko, A.; Dahm, T.; Troll, V.R.; Tilmann, F.; et al. Complex hazard cascade culminating in the Anak Krakatau sector collapse. *Nat. Commun.* **2019**, *10*, 4339. [CrossRef]
61. Rotta, L.H.S.; Alcantara, E.; Park, E.; Negri, R.G.; Lin, Y.N.; Bernardo, N.; Mendes, T.S.G.; Filho, C.R.S. The 2019 Brumadinho tailings dam collapse: Possible cause and impacts of the worst human and environmental disaster in Brazil. *Int. J. Appl. Earth Obs. Geoinf.* **2020**, *90*, 102119. [CrossRef]
62. Cordeiro, M.C.; Garcia, G.D.; Rocha, A.M.; Tschoeke, D.A.; Campeao, M.E.; Appolinario, L.R.; Soares, A.C.; Leomil, L.; Froes, A.; Bahiense, L.; et al. Insights on the freshwater microbiomes metabolic changes associated with the world's largest mining disaster. *Sci. Total Environ.* **2019**, *654*, 1209–1217. [CrossRef] [PubMed]
63. Queiroz, H.M.; Nobrega, G.N.; Ferreira, T.O.; Almeida, L.S.; Romero, T.B.; Santaella, S.T.; Bernardino, A.F.; Otero, X.L. The Samarco mine tailing disaster: A possible time-bomb for heavy metals contamination? *Sci. Total Environ.* **2018**, *637–638*, 498–506. [CrossRef] [PubMed]
64. ESA. Path of Mudflow after Dam Failure. Available online: https://en.wikipedia.org/wiki/Brumadinho_dam_disaster#/media/File:Brumadinho_dam_catastrophy_2.jpg (accessed on 17 August 2019).
65. Comiti, F.; Mao, L.; Wilcox, A.; Wohl, E.E.; Lenzi, M.A. Field-derived relationships for flow velocity and resistance in high-gradient streams. *J. Hydrol.* **2007**, *340*, 48–62. [CrossRef]
66. Liljegren, L. The effect of a mean fluid velocity gradient on the streamwise velocity variance of a particle suspended in a turbulent flow. *Int. J. Multiph. Flow* **1993**, *19*, 471–484. [CrossRef]
67. Huang, H.B.; Ma, H.Z.; Sha, Z.J.; Cao, G.C.; Ou, L.Y.; Yang, H.Z. Research of distribution of suspended sediments in Longyangxia reservoir based on RS. *J. Salt Lake Res.* **2004**, *12*, 34–37.
68. Kumar, V.; Garg, R.D. Comparison of different mapping techniques for classifying hyperspectral data. *J. Indian Soc. Remote Sens.* **2012**, *40*, 411–420. [CrossRef]
69. Zhang, H.K.; Roy, D.P. Computationally inexpensive Landsat 8 Operational Land Imager (OLI) pansharpening. *Remote Sens.* **2016**, *8*, 180. [CrossRef]
70. Fatemi, S.B.; Gholinejad, S. Assessing the effectiveness of Google Earth images for spatial enhancement of rapidEye multi-spectral imagery. *Int. J. Remote Sens.* **2019**, *40*, 4526–4543. [CrossRef]
71. Delleji, T.; Kallel, A.; Hamida, A.B. Iterative scheme for MS image pansharpening based on the combination of multi-resolution decompositions. *Int. J. Remote Sens.* **2016**, *37*, 6041–6075. [CrossRef]
72. Guo, Q.; Chen, S.; Leung, H.; Liu, S. Covariance intersection based image fusion technique with application to pansharpening in remote sensing. *Inf. Sci.* **2010**, *180*, 3434–3443. [CrossRef]
73. Vale. Clarifications Regarding Dam I of the Córrego do Feijão Mine. Available online: http://www.vale.com/brasil/EN/aboutvale/news/Pages/Clarifications-regarding-Dam-I-of-the-Corrego-do-Feijao-Mine.aspx (accessed on 18 April 2019).
74. Fernandes, G.W.; Goulart, F.F.; Ranieri, B.D.; Coelho, M.S.; Dales, K.; Boesche, N.; Bustamante, M.; Carvalho, F.A.; Carvalho, D.C.; Dirzo, R.; et al. Deep into the mud: Ecological and socio-economic impacts of the dam breach in Mariana, Brazil. *Nat. Conserv.* **2016**, *14*, 35–45. [CrossRef]
75. Francini-Filho, R.B.; Cordeiro, M.C.; Omachi, C.Y.; Rocha, A.M.; Bahiense, L.; Garcia, G.D.; Tschoeke, D.; de Almeida, M.G.; Rangel, T.P.; De Oliveira, B.C.V.; et al. Remote sensing, isotopic composition and metagenomics analyses revealed Doce River ore plume reached the southern Abrolhos Bank Reefs. *Sci. Total Environ.* **2019**, *697*, 134038. [CrossRef] [PubMed]
76. Festin, E.S.; Tigabu, M.; Chileshe, M.N.; Syampungani, S.; Odén, P.C. Progresses in restoration of post-mining landscape in Africa. *J. For. Res.* **2018**, *30*, 381–396. [CrossRef]
77. Robertson, P.K.; da Fonseca, A.V.; Ulrich, B.; Coffin, J. Characterization of unsaturated mine waste: A case history. *Can. Geotech. J.* **2017**, *54*, 1752–1761. [CrossRef]
78. Yu, G.; Song, C.; Pan, Y.; Li, L.; Li, R.; Lu, S. Review of new progress in tailing dam safety in foreign research and current state with development trent in China. *Chin. J. Rock Mech. Eng.* **2014**, *33*, 3238–3248.
79. Agurto-Detzel, H.; Bianchi, M.; Assumpção, M.; Schimmel, M.; Collaço, B.; Ciardelli, C.; Barbosa, J.R.; Calhau, J. The tailings dam failure of 5 November 2015 in SE Brazil and its preceding seismic sequence. *Geophys. Res. Lett.* **2016**, *43*, 4929–4936. [CrossRef]
80. Fourie, A.; Blight, G.; Papageorgiou, G. Static liquefaction as a possible explanation for the Merriespruit tailings dam failure: Reply. *Can. Geotech. J.* **2002**, *39*, 1441. [CrossRef]
81. Kossoff, D.; Dubbin, W.; Alfredsson, M.; Edwards, S.; Macklin, M.; Hudson-Edwards, K.A. Mine tailings dams: Characteristics, failure, environmental impacts, and remediation. *Appl. Geochem.* **2014**, *51*, 229–245. [CrossRef]
82. Cardinali, M.; Galli, M.; Guzzetti, F.; Ardizzone, F.; Reichenbach, P.; Bartoccini, P. Rainfall induced landslides in December 2004 in south-western Umbria, central Italy: Types, extent, damage and risk assessment. *Nat. Hazards Earth Syst. Sci.* **2006**, *6*, 237–260. [CrossRef]

83. Cui, P.; Dang, C.; Zhuang, J.-q.; You, Y.; Chen, X.-q.; Scott, K.M. Landslide-dammed lake at Tangjiashan, Sichuan province, China (triggered by the Wenchuan Earthquake, May 12, 2008): Risk assessment, mitigation strategy, and lessons learned. *Environ. Earth Sci.* **2010**, *65*, 1055–1065. [CrossRef]
84. Cui, P.; Zou, Q.; Xiang, L.-z.; Zeng, C. Risk assessment of simultaneous debris flows in mountain townships. *Prog. Phys. Geogr. Earth Environ.* **2013**, *37*, 516–542. [CrossRef]
85. Lu, P.; Catani, F.; Tofani, V.; Casagli, N. Quantitative hazard and risk assessment for slow-moving landslides from Persistent Scatterer Interferometry. *Landslides* **2013**, *11*, 685–696. [CrossRef]
86. Globo, O. Empresas Envolvidas em Desastres Ambientais Quitaram só 3.4% de R$785 Milhões em Multas. Available online: https://oglobo.globo.com/economia/empresas-envolvidas-em-desastres-ambientais-quitaram-so-34-de-785-milhoes-em-multas-22657874 (accessed on 18 April 2019).
87. Guardian, T. 'That's Going to Burst': Brazilian Dam Workers Say They Warned of Disaster. Available online: https://www.theguardian.com/world/2019/feb/06/brazil-dam-collapse-workers-say-they-warned-owners (accessed on 17 August 2019).
88. Agricolax. Schematic Cross Section Showing Design of Failed Dam. Available online: https://en.wikipedia.org/wiki/Brumadinho_dam_disaster#/media/File:Brumadinho_dam_-_cross_section_-_en.png (accessed on 14 October 2019).
89. AGU-Blogosphere. Brumadinho Disaster: The Extent of the Environmental Impact. Available online: https://blogs.agu.org/landslideblog/page/13/ (accessed on 23 October 2019).
90. World-Weather-Online. Brumadinho Historical Weather. World Weather Online. Available online: https://www.worldweatheronline.com/brumadinho-weather-history/minas-gerais/br.aspx (accessed on 17 August 2019).
91. NOAA. What are El Niño and La Niña? Available online: https://oceanservice.noaa.gov/facts/ninonina.html (accessed on 17 October 2020).
92. Barnston, A. How ENSO Leads to a Cascade of Global Impacts. Available online: https://www.climate.gov/news-features/blogs/enso/how-enso-leads-cascade-global-impacts (accessed on 17 August 2019).
93. IRI. What Changes in Rainfall are Typical during ei Niño? Available online: http://iridl.ldeo.columbia.edu/maproom/IFRC/FIC/elninorain.html (accessed on 17 August 2019).
94. IRI. Are the Next 3 Months Likely to be Unusually Wet or Dry? Available online: http://iridl.ldeo.columbia.edu/maproom/IFRC/FIC/prcp_fcst.html?F=Oct%202018&L=2 (accessed on 17 August 2019).
95. Hatje, V.; Pedreira, R.M.A.; de Rezende, C.E.; Schettini, C.A.F.; de Souza, G.C.; Marin, D.C.; Hackspacher, P.C. The environmental impacts of one of the largest tailing dam failures worldwide. *Sci. Rep.* **2017**, *7*, 10706. [CrossRef] [PubMed]
96. de Carvalho, D.W. The ore tailings dam rupture disaster in Mariana, Brazil 2015: What we have to learn from anthropogenic disasters. *Nat. Resour. J.* **2019**, *59*, 281.
97. Adiansyah, J.S.; Rosano, M.; Vink, S.; Keir, G. A framework for a sustainable approach to mine tailings management: Disposal strategies. *J. Clean. Prod.* **2015**, *108*, 1050–1062. [CrossRef]
98. Laasonen, M.J. European Working Group "Management of dam incidents" Case study: Finland. In Proceedings of the International Symposium on Dams in a Global Environmental Challenges, Bali, Indonesia, 1–6 June 2014.
99. Balaniuk, R.; Isupova, O.; Reece, S. Mining and tailings dam detection in satellite imagery using deep learning. *Sensors* **2020**, *20*, 6936. [CrossRef]
100. Wu, J.; Wu, Y.; Lu, J.; Lee, L. Field investigations and laboratory simulation of clogging in Lixi tailings dam of Jinduicheng, China. *Environ. Geol.* **2007**, *53*, 387–397.
101. Mulligan, M.; van Soesbergen, A.; Sáenz, L. GOODD, a global dataset of more than 38,000 georeferenced dams. *Sci. Data* **2020**, *7*, 1–8. [CrossRef]
102. Blanchard, B.S. *System Engineering Management*; John Wiley & Sons: Hoboken, NJ, USA, 2004.
103. Blanchard, B.S.; Fabrycky, W.J.; Fabrycky, W.J. *Systems Engineering and Analysis*; Prentice Hall: Englewood Cliffs, NJ, USA, 1990; Volume 4.
104. Yang, Y.; Wei, Z.; Cao, G.; Yang, Y.; Wang, H.; Zhuang, S.; Lu, T. A case study on utilizing geotextile tubes for tailings dams construction in China. *Geotext. Geomembr.* **2019**, *47*, 187–192. [CrossRef]
105. Wei, Z.; Yin, G.; Wang, J.-G.; Wan, L.; Li, G. Design, construction and management of tailings storage facilities for surface disposal in China: Case studies of failures. *Waste Manag. Res.* **2013**, *31*, 106–112. [CrossRef]
106. Wang, K.; Yang, P.; Hudson-Edwards, K.A.; Lyu, W.; Yang, C.; Jing, X. Integration of DSM and SPH to model tailings dam failure run-Out slurry routing across 3D real terrain. *Water* **2018**, *10*, 1087. [CrossRef]
107. Yin, G.; Li, G.; Wei, Z.; Wan, L.; Shui, G.; Jing, X. Stability analysis of a copper tailings dam via laboratory model tests: A Chinese case study. *Miner. Eng.* **2011**, *24*, 122–130. [CrossRef]
108. Li, M. Ecological restoration of mineland with particular reference to the metalliferous mine wasteland in China: A review of research and practice. *Sci. Total Environ.* **2006**, *357*, 38–53. [CrossRef]
109. Aires, U.R.V.; Santos, B.S.M.; Coelho, C.D.; da Silva, D.D.; Calijuri, M.L. Changes in land use and land cover as a result of the failure of a mining tailings dam in Mariana, MG, Brazil. *Land Use Policy* **2018**, *70*, 63–70. [CrossRef]
110. Xin, Z.; Xiaohu, X.; Kaili, X. Study on the risk assessment of the tailings dam break. *Procedia Eng.* **2011**, *26*, 2261–2269. [CrossRef]
111. Buch, A.C.; Niemeyer, J.C.; Marques, E.D.; Silva-Filho, E.V. Ecological risk assessment of trace metals in soils affected by mine tailings. *J. Hazard. Mater.* **2020**, *403*, 123852. [CrossRef]

112. Li, W.; Ye, Y.; Hu, N.; Wang, X.; Wang, Q. Real-time warning and risk assessment of tailings dam disaster status based on dynamic hierarchy-grey relation analysis. *Complexity* **2019**, *2019*, 5873420. [CrossRef]
113. Kiventerä, J.; Golek, L.; Yliniemi, J.; Ferreira, V.; Deja, J.; Illikainen, M. Utilization of sulphidic tailings from gold mine as a raw material in geopolymerization. *Int. J. Miner. Process.* **2016**, *149*, 104–110. [CrossRef]
114. Choi, Y.W.; Kim, Y.J.; Choi, O.; Lee, K.M.; Lachemi, M. Utilization of tailings from tungsten mine waste as a substitution material for cement. *Constr. Build. Mater.* **2009**, *23*, 2481–2486.
115. Bakken, A.; Gautneb, H.; Sveistrup, T.; Myhr, K. Crushed rocks and mine tailings applied as K fertilizers on grassland. *Nutr. Cycl. Agroecosystems* **2000**, *56*, 53–57. [CrossRef]
116. Ballesteros, E.R.; Ramírez, M.H. Identity and community—Reflections on the development of mining heritage tourism in Southern Spain. *Tour. Manag.* **2007**, *28*, 677–687. [CrossRef]
117. Chon, K.-S.; Evans, M.R. Tourism in a rural area—A coal mining-county experience. *Tour. Manag.* **1989**, *10*, 315–321. [CrossRef]
118. Ćopić, S.; ĐorđevićA, J.; Lukić, T.; Stojanović, V.; Đukičin, S.; Besermenji, S.; Stamenković, I.; Tumarić, A. Transformation of industrial heritage: An example of tourism industry development in the Ruhr area (Germany). *Geogr. Pannonica* **2014**, *18*, 43–50. [CrossRef]
119. Wang, K.; Tang, C.; Liu, J. A measuring model on tourist satisfaction index in cultural creative-type tourism destination—A case of 798 Art Zone in Beijing. *Tour. Trib. Lvyou Xuekan* **2011**, *26*, 36–44.